Int. J. Heat Mass Transfer. Vol. 35, No. 5, pp. 1035–1048, 1992
Printed in Great Britain

0017–9310/92 $5.00 + 0.00
Pergamon Press Ltd

An analytical model of spray combustion for slowly moving fuel drops

D. SANYAL and T. SUNDARARAJAN
Department of Mechanical Engineering, Indian Institute of Technology, Kanpur 208016, India

(*Received* 13 *June* 1990 *and in final form* 20 *May* 1991)

Abstract—The combustion of a dilute fuel spray has been analysed in the framework of the spherical cell model. The quasi-steady burning of a typical droplet has been studied using the thin-flame approximation. At the cell surface, the boundary conditions of zero shear stress and convective heat/mass transport have been imposed. Analytical solutions for creeping motion of the drop have been obtained through a regular perturbation procedure with the drop Reynolds number as the perturbation parameter. A parametric study involving the drop Reynolds number, cell size and the free-stream conditions outside the cell surface has also been carried out.

INTRODUCTION

COMBUSTION of fuel droplets has been a subject of study for the past four decades. The majority of available analyses pertain to the spherically symmetric combustion of an isolated droplet in a stationary oxidizing environment [1–4]. Faeth [4] has also reviewed the studies which approximately estimate the convective enhancement in the burning rate. The influence of drop motion has been examined in detail over a wide Reynolds number range in the analyses of evaporation [5–7], whereas theoretical investigations dealing with droplet combustion have been confined to the creeping flow regime. The singular perturbation technique was adopted [8, 9] to analyse the burning of an isolated drop moving slowly through an infinite expanse of an oxidizing atmosphere. An approximate accounting of convective effects was introduced by Sangiovanni [10], who considered the heat and mass transfer during combustion to be confined to a film adjacent to the drop. The thickness of the convective film was evaluated from suitable Nusselt number correlations.

Studies involving the interaction between burning drops are of recent origin. These analyses are broadly based on two alternative approaches, namely the group combustion model and the discrete droplet burning model. In the group combustion formulation [11–13], attention is primarily focussed on the collective burning effects of a cloud of droplets. A more detailed picture of the burning characteristics in the vicinity of any typical droplet is revealed by the discrete droplet burning approach. It was suggested by Chiu and Liu [12] that a characteristic group combustion number, G, can be utilized to demarcate the regimes of applicability of the two aforementioned models.

In the discrete droplet burning formulation, each drop is considered as a fuel source as well as a heat sink. Brzustowski *et al.* [14] used bispherical coordinates for calculating the interaction of two burning droplets. Labowsky [15–17] modified the principle of superposition to obtain the solution pertaining to a number of simple arrangements of droplets. Ray and Davis [18] carried out a transient analysis of the multi-droplet combustion utilizing the Fourier transform technique. Marberry *et al.* [19] applied an approximate mass balance equation containing a delta function and developed a much simpler solution procedure capable of reproducing the results of earlier calculations [14–17]. However, all these studies failed to account for drop motion, due to the apparent mathematical difficulties arising from the inclusion of convective terms. Furthermore, the analyses conducted so far were limited to simple droplet arrays.

A powerful approach which has met with spectacular success in the hydrodynamic analysis of multi-particle systems is the unit cell approach [20, 21]. In this approach, the spray is considered to be divided into many cells, each of which contains a particle placed at its centre. The cells are isolated from each other by applying suitable boundary conditions at the cell surfaces. Thus, the complex multi-body spray problem greatly simplifies to the study of a representative unit cell. Both Happel [20] and Kuwabara [21] investigated creeping motion of a particle assemblage through a fluid. Happel employed a zero shear stress condition at the cell boundary with the objective of conceptually isolating the cells from mutual energy exchange. However, the zero vorticity condition of Kuwabara was presented as a hypothesis lacking such a physical basis. Later, the cell model was also utilized [22–24] in transient analyses of evaporating, stationary droplets. Zung [22] investigated a purely mass transfer problem, while Tishkoff [23] also considered the heat transfer aspect. To achieve cell isolation, a zero mass transfer condition was imposed by Zung, whereas an additional zero heat flux condition was employed by Tishkoff. In all the models discussed in refs. [20–23], the cell voidage was assumed to be equal

NOMENCLATURE

C_p	specific heat at constant pressure
D	diffusion coefficient of the gas phase
G	Schvab–Zeldovich variable, equation (2a)
H	Schvab–Zeldovich variable, equation (2b)
h	enthalpy (with letter subscripts); heat transfer coefficient
Δh_c	heat of combustion
I_{p_n}	polynomial defined as $\int_1^\mu P_n(\mu)\,\mathrm{d}\mu$
L	latent heat of evaporation
Nu	Nusselt number, hr_d/λ
P_n	Legendre polynomial of order n
r	radius
$\bar{R}$	universal gas constant
Re	Reynolds number, $\rho u_\infty r_d/\eta$
Sc	Schmidt number of the gas phase
u	velocity component (when subscripted with letters), velocity coefficient (when subscripted with number)
v_0	coefficient equal to $Sc \cdot u_0$
W	molecular weight
Y	modified mass fraction
$\bar{Y}$	mass fraction.

Greek symbols

η	viscosity
θ	angular coordinate
λ	conductivity of the gas mixture
μ	coordinate variable equal to $\cos\theta$
ν	stoichiometric coefficient
ξ	normalized radial coordinate
ρ	density
τ	shear stress
Ψ	stream function for the gas phase
$\hat{\Psi}$	stream function for the liquid phase.

Subscripts

B	boiling point of the fuel
c	cell surface
d	droplet surface
F	fuel
P	product
wb	wet bulb
X	oxidizer
0	zero order quantity
1	first order quantity
10	first order quantity associated with zero order Legendre polynomial
11	first order quantity associated with first order Legendre polynomial
∞	cloud condition.

Superscript

0	reference quantity.

to the system voidage. However, Bellan and Cuffel [24] considered spherical cells to be touching each other. Heat and mass transfer in the intercellular space was accounted for by adding suitable terms in the global conservation equations.

In the present work, the unit cell approaches due to Happel [20] and Bellan and Cuffel [24] have been modified for the analysis of combustion of a dilute spray. The region of the spray sufficiently away from the injector, in a typical gas turbine combustor, is characterized by droplets separated from each other by distances substantially larger in comparison to the droplet diameters. Under such a condition, the assumption of a dilute spray burning is justified. The creeping flow regime of drop motion is examined, since the atomized fuel drops are often very small in size. The small value of the Reynolds number, coupled with the finite size of the cell, renders the problem amenable to regular perturbation study, with the Reynolds number as the perturbation parameter. An analytical solution is developed in this paper for the quasi-steady burning of a droplet within a spherical cell. A detailed parametric study of the results obtained from the analytical solution is also presented.

MATHEMATICAL FORMULATION OF THE PROBLEM

A dilute spray of single component fuel drops moving steadily through an oxidizing atmosphere is considered. The discrete droplet burning model is adopted, owing to the smallness of the group combustion number for a dilute spray. Following the unit cell approach, the analysis focuses attention on a typical droplet inside a concentric spherical cell (Figs. 1(a) and (b)). The spray is conceived to be made up of contiguous cells located in a common convective cloud. This description of the spray is very similar to the one propounded by Bellan and Cuffel [24]. The convective cloud brings in the necessary oxygen supply and takes away the products of combustion and heat from each cell as it flows through the intercellular space. For a uniformly distributed spray of drops, the cross-sectional area normal to the direction of droplet motion varies periodically, resulting in a similar variation of relative flow velocity. The composition and temperature of the cloud depend on the overall burning characteristics of the spray. However, in the present work, these are taken as prescribed conditions. The combustion process within the cell is proposed to

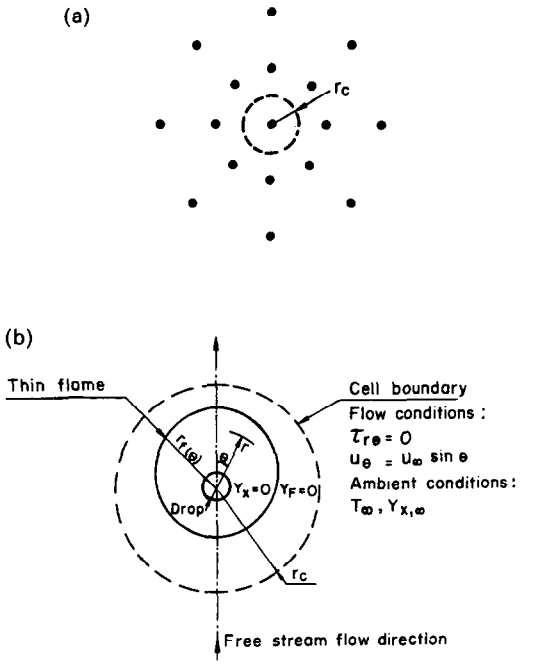

FIG. 1. (a) Spray of droplets. (b) A typical droplet in a cell.

be axisymmetric about the direction of drop translation. A coordinate system (r, θ), fixed to the drop centre, is considered (Fig. 1(b)). The other important assumptions include the thin-flame approximation, unit gas-phase Lewis number, constant properties and quasi-steady burning, which are usually invoked in any theoretical study of combustion. The imposition of quasi-steady burning of the droplet inside the cell is reasonable as long as the spray is dilute. Also, in a dilute spray, the chances of inter-droplet collisions and associated complexities are less. Buoyancy effects have been neglected in the present study due to the small size of droplets. The liquid phase heating is assumed to have been completed and the entire drop is taken to be at the corresponding wet bulb temperature, T_{wb}. Subject to the above assumptions, the dimensionless governing equations [9, 25] in terms of the stream function and Schvab–Zeldovich variables are given below.

The liquid phase flow equation is

$$E^2E^2\hat{\Psi} - (1-\mu^2)\frac{\partial\hat{\Psi}}{\partial r}\frac{\partial}{\partial\mu}\left\{\frac{E^2\hat{\Psi}}{r^2(1-\mu^2)}\right\} + \frac{\partial\hat{\Psi}}{\partial\mu}\frac{\partial}{\partial r}\left(\frac{E^2\hat{\Psi}}{r^2}\right) = 0, \quad r < 1. \quad (1a)$$

Gas phase flow is governed by

$$E^2E^2\Psi - (1-\mu^2)\frac{\partial\Psi}{\partial r}\frac{\partial}{\partial\mu}\left\{\frac{E^2\Psi}{r^2(1-\mu^2)}\right\} + \frac{\partial\Psi}{\partial\mu}\frac{\partial}{\partial r}\left(\frac{E^2\Psi}{r^2}\right) = 0, \quad 1 < r < r_c. \quad (1b)$$

The gas phase heat and mass transport equations can be expressed as

$$\frac{\partial}{\partial r}\left(r^2\frac{\partial G}{\partial r}\right) + \frac{\partial}{\partial\mu}\left\{(1-\mu^2)\frac{\partial G}{\partial\mu}\right\} + Sc\left(\frac{\partial\Psi}{\partial\mu}\frac{\partial G}{\partial r} - \frac{\partial\Psi}{\partial r}\frac{\partial G}{\partial\mu}\right) = 0, 1 < r < r_c \quad (1c)$$

and

$$\frac{\partial}{\partial r}\left(r^2\frac{\partial H}{\partial r}\right) + \frac{\partial}{\partial\mu}\left\{(1-\mu^2)\frac{\partial H}{\partial\mu}\right\} + Sc\left(\frac{\partial\Psi}{\partial\mu}\frac{\partial H}{\partial r} - \frac{\partial\Psi}{\partial r}\frac{\partial H}{\partial\mu}\right) = 0, 1 < r < r_c. \quad (1d)$$

In the above equations

$$E^2 = \frac{\partial^2}{\partial r^2} + \frac{1-\mu^2}{r^2}\frac{\partial^2}{\partial\mu^2}$$

and $\mu = \cos\theta$.

Also, Ψ and $\hat{\Psi}$ are the stream functions corresponding to the gas and liquid phases respectively and G and H are the Schvab–Zeldovich variables (henceforth called S–Z variables) defined as

$$G = Y_F - Y_X \quad (2a)$$

and

$$H = T - Y_X. \quad (2b)$$

Reference quantities for non-dimensionalizing length, stream function, temperature and mass fractions of fuel and oxidizer are respectively chosen as r_d, $r_d\eta/\rho$, $\Delta h_c/C_pW$, $(-\nu_F W_F/W)$ and $(-\nu_X W_X/W)$, where

$$W = \nu_F W_F + \nu_X W_X$$

and

$$\Delta h_c = \nu_F W_F h_F^\circ + \nu_X W_X h_X^\circ - \nu_p W_p h_p^\circ.$$

The boundary conditions for equations (1a)–(1d) are given as follows.

(i) Continuity of tangential velocity and shear stress at the drop surface require

$$\left.\frac{\partial\hat{\Psi}}{\partial r}\right|_{r=1} = \left.\frac{\partial\Psi}{\partial r}\right|_{r=1} \quad (3a)$$

and

$$\left[\frac{\partial^2\hat{\Psi}}{\partial r^2} - 2\frac{\partial\hat{\Psi}}{\partial r} - (1-\mu^2)\frac{\partial^2\hat{\Psi}}{\partial\mu^2}\right]_{r=1} = \phi_\eta\left[\frac{\partial^2\Psi}{\partial r^2} - 2\frac{\partial\Psi}{\partial r} - (1-\mu^2)\frac{\partial^2\Psi}{\partial\mu^2}\right]_{r=1} \quad (3b)$$

where ϕ_η is the ratio of gas phase and liquid phase viscosities.

(ii) Since the density ratio between the liquid and gas phases is large, one obtains from the mass balance at the interface that

$$\left.\frac{\partial \Psi}{\partial \mu}\right|_{r=1} \cong 0. \tag{3c}$$

(iii) The heat and mass transfer conditions at the interface can be expressed as

$$\left.\frac{\partial G}{\partial r}\right|_{r=1} - Sc\, u_d G|_{r=1} = -Sc\, \alpha_F u_d \tag{3d}$$

and

$$\left.\frac{\partial H}{\partial r}\right|_{r=1} = Sc\, L u_d \tag{3e}$$

where u_d is the rate of evaporation from the drop surface and $\alpha_F = -W/\nu_F W_F$.

(iv) The Clausius–Clapeyron equation gives

$$G|_{r=1} = \alpha_F \exp\left[\beta\left(\frac{1}{T_B} - \frac{1}{H}\right)\right]\Bigg|_{r=1} \tag{3f}$$

where $\beta = (W W_F L C_p)/(\bar{R}\Delta h_c)$.

(v) In compliance with Happel's free-surface cell model, the shear stress at the cell surface is set equal to zero. Therefore

$$\left[\frac{\partial^2 \psi}{\partial r^2} - \frac{2}{r_c}\frac{\partial \Psi}{\partial r} - \frac{1-\mu^2}{r_c^2}\frac{\partial^2 \Psi}{\partial \mu^2}\right]\Bigg|_{r=r_c} = 0. \tag{3g}$$

(vi) It has been described earlier that the cloud flow velocity varies periodically for a regularly spaced array of drops. For this reason, a tangential velocity condition of the form

$$\left(\frac{1}{r\sin\theta}\frac{\partial \Psi}{\partial r}\right)\Bigg|_{r=r_c} = Re\sin\theta \tag{3h}$$

is imposed at the cell boundary, where the Reynolds number Re is based on the maximum velocity of the cloud flow. Such a periodic pattern along the cell boundaries was in fact predicted by Gal-or and Waslo [26].

(viii) Convective heat and mass transport between the cloud and the cell is considered in the present work. In earlier transient analyses [22, 23], the heat and mass fluxes at the cell surface were taken to be zero. However, these conditions do not fulfil the requirements of the quasi-steady model. Moreover, neither concentration nor temperature at the cell surface are known a priori and prescribing these would strongly influence the burning characteristics of the drop. Therefore, convective boundary conditions, which are likely to have lesser bearing upon the temperature and concentration fields inside the cell, are applied at the cell boundary. In terms of S–Z variables, these conditions can be expressed as

$$\left.\frac{\partial G}{\partial r}\right|_{r=r_c} + \left(Nu - \frac{Sc}{r_c^2}u_d\right)G\Big|_{r=r_c} = -\left(Nu - \frac{Sc}{r_c^2}u_d\right)Y_{X,\infty} \tag{3i}$$

and

$$\left.\frac{\partial H}{\partial r}\right|_{r=r_c} + \left(Nu - \frac{Sc}{r_c^2}u_d\right)H\Big|_{r=r_c} = \left(Nu - \frac{Sc}{r_c^2}u_d\right)(T_\infty - Y_{X,\infty}). \tag{3j}$$

The above form of cell boundary conditions have been chosen keeping in mind that convective effects arise both due to the drop motion and the radial flow generated by combustion. It is evident that the Nusselt number Nu should depend on factors such as droplet arrangement, fluid properties and flow characteristics. The selection of an appropriate value for this parameter is discussed later.

SOLUTION PROCEDURE

A careful examination of the physical features of the problem reveals that there are two independent flow effects, one generated by the combustion process itself and the other due to free and forced convection around the droplet. For a small stationary drop, the problem reduces to that of spherically symmetric burning and a purely radial flow occurs in this case. For a translating drop, the flow field no longer remains radial. In the present work, the buoyancy-driven flow is neglected and the convective flow generated by drop motion is considered to be weak in comparison to the radial flow caused by burning. This requirement is met if the Reynolds number of drop motion is very small ($Re = \rho u_\infty r_d/\eta \ll 1$), since the radial velocity generated by combustion is $O(D/r_d)$ and the Schmidt number of the gas phase is $O(1)$. The small Re assumption enables us to adopt a perturbation scheme for obtaining the solution. Indeed, a uniformly valid regular perturbation expansion is appropriate for the multi-drop situation, since the solution domain is finite in extent. Such an analysis has been carried out by El-Kaissy and Homsy [27] for flow through a multi-particle assemblage. The authors have also shown that this scheme is valid for a larger solution domain at a smaller Re and vice versa.

With the above-mentioned ideas in mind, the unknown variables can be expanded in the forms:

$$\Psi(r,\mu) = Re\,\Psi_1(r,\mu) + o(Re) \tag{4a}$$

$$\Psi(r,\mu) = \Psi_0(\mu) + Re\,\Psi_1(r,\mu) + o(Re) \tag{4b}$$

$$G(r,\mu) = G_0(r) + Re\,G_1(r,\mu) + o(Re) \tag{4c}$$

$$H(r,\mu) = H_0(r) + Re\,H_1(r,\mu) + o(Re). \tag{4d}$$

In addition, since the drop motion augments heat and mass transfer rates above the values corresponding to the basic radial flow, the quantities u_d and Nu may be expanded as

$$u_d(\mu) = u_0 + Re\,u_1(\mu) + o(Re) \tag{4e}$$

$$Nu = Nu_0 + Re\,Nu_1 + o(Re). \tag{4f}$$

For the sake of mathematical simplicity, the expansions have been truncated at the first order.

The Nusselt number at the cell surface is a free paramcter of the present model, whose value needs to be appropriately determined. In conformity with equation (4f), this parameter is evaluated as

$$Nu = Nu_0[1+0.5\,Sc\,Re(r_c/r_d)] \tag{4g}$$

where Nu_0 is the Nusselt number in the absence of drop motion. The augmentation factor, pertaining to the motion of the drop, has been selected in the form which is commonly used for a creeping flow regime [4, 28]. Due care has been taken to account for the fact that the convective condition of the present formulation is applied at the cell surface. The procedure of estimating the zero order Nusselt number Nu_0 has been described in Appendix A.

Zero order solutions

The zero order problem corresponds to spherically symmetric burning of the drop inside the cell, with a purely radial flow emanating from the drop surface. Continuity of mass flux for this spherically symmetric situation leads to

$$\rho u_r 4\pi r^2 = \text{constant} \tag{5a}$$

where u_r is the zero order radial flow velocity. For constant-density flow, the above expression can be recast in the form

$$u_r = u_0/r^2 \tag{5b}$$

where u_0 is the zero order evaporation velocity at $r = 1$, as described in equation (4e). The corresponding zero order stream function solution is

$$\Psi_0 = u_0(1-\mu). \tag{6}$$

From equations (1c) and (d), the zero order equations for the S–Z variables are obtained as

$$(r^2G_0')' - v_0G_0' = 0, \quad 1 < r < r_c \tag{7a}$$

and

$$(r^2H_0')' - v_0H_0' = 0, \quad 1 < r < r_c \tag{7b}$$

where $v_0 = Sc\,u_0$, and the prime denotes differentiation with respect to r. The general solutions for the above equations are

$$G_0 = A_{g_0}(e^{-v_0/r} - e^{-v_0})/v_0 + B_{g_0} \tag{8a}$$

and

$$H_0 = A_{h_0}(e^{-v_0/r} - e^{-v_0})/v_0 + B_{h_0} \tag{8b}$$

where A_{g_0}, A_{h_0}, B_{g_0} and B_{h_0} are the constants of integration.

The zero order boundary conditions derived from equations (3d)–(3f), (3i) and (3j) are:

$$G_0'(1) - v_0G_0(1) = -\alpha_F v_0 \tag{9a}$$

$$H_0'(1) = Lv_0 \tag{9b}$$

$$G_0'(r_c) + (Nu_0 - v_0/r_c^2)G_0(r_c) = -(Nu_0 - v_0/r_c^2)Y_{X,\infty} \tag{9c}$$

$$H_0'(r_c) + (Nu_0 - v_0/r_c^2)H_0(r_c) = (Nu_0 - v_0/r_c^2)(T_\infty - Y_{X,\infty}) \tag{9d}$$

$$\ln\frac{G_0(1)}{\alpha_F} = \beta\left\{\frac{1}{T_B} - \frac{1}{H_0(1)}\right\}. \tag{9e}$$

The above relations can be used to determine the constants of integration and the spherically symmetric evaporation velocity, u_0. Finally, the complete zero order solutions for S–Z variables are obtained as

$$G_0(r) = \alpha_F - \frac{1}{Nu_0}(\alpha_F + Y_{X,\infty})\left(Nu_0 - \frac{v_0}{r_c^2}\right) \times \exp\left\{v_0\left(\frac{1}{r_c} - \frac{1}{r}\right)\right\} \tag{10a}$$

and

$$H_0(r) = T_\infty - Y_{X,\infty} + L\left[\exp\left\{v_0\left(1-\frac{1}{r}\right)\right\} - Nu_0\exp\{v_0(1-1/r_c)\}\{Nu_0 - v_0/r_c^2\}^{-1}\right] \tag{10b}$$

where $v_0 (= Sc\,u_0)$ can be iteratively determined through the equation

$$\ln\left[1 - \left(1 + \frac{Y_{X,\infty}}{\alpha_F}\right)\left(1 - \frac{v_0}{Nu_0 r_c^2}\right) \times \exp\left\{-v_0\left(1-\frac{1}{r_c}\right)\right\}\right] = \beta\left[\frac{1}{T_B} - \frac{1}{T_\infty - Y_{X,\infty} + L\left\{1 - \left[\frac{Nu_0\exp(v_0 - v_0/r_c)}{(Nu_0 - v_0/r_c^2)}\right]\right\}}\right]. \tag{10c}$$

First order solutions

The first order stream function equations for the liquid and gas phases respectively are

$$E^2E^2\hat{\Psi}_1 = 0, \quad r < 1 \tag{11a}$$

and

$$E^2E^2\Psi_1 = \frac{u_0}{r^2}\left(\frac{\partial}{\partial r} - \frac{2}{r}\right)E^2\Psi_1, \quad 1 < r < r_c. \tag{11b}$$

Following refs. [9, 29], the general solution of the above equations can be obtained as:

$$\hat{\Psi}_1 = \sum_{n=1}^{\infty}(\hat{c}_{n1}r^{n+3} + \hat{c}_{n2}r^{n+1} + \hat{c}_{n3}r^{-n+2} + \hat{c}_{n4}r^{-n})I_{P_n}(\mu) \tag{12a}$$

and

$$\Psi_1 = \left[c_0 I_{P_0}(\mu) + \{c_{11} r^4 + c_{12} r^2 + c_{13}/r + c_{14} I_\Psi(r)\} I_{P_1}(\mu) + \sum_{n=2}^{\infty} c_n f_n(r) I_{P_n}(\mu) \right] \quad (12b)$$

where

$$I_{P_n}(\mu) = \int_1^\mu P_n(\mu)\, d\mu$$

$$I_\Psi(r) = \frac{u_0}{r} \int_{1/u_0}^{r/u_0} e^{-1/\eta} (\eta^4 + \eta^3)\, d\eta$$

and $f_n(r)$, in general, is made up of four independent radial solutions.

The constants of integration in the above equations can be determined from the first order boundary conditions derived from equations (3a), (3b), (3g) and (3h). Among these, radial velocity condition at the drop surface and the convective velocity condition at the cell surface merit special attention. To first order in Re, the conditions are

$$\left.\frac{\partial \Psi_1}{\partial \mu}\right|_{r=1} = -u_1(\mu) \quad (13a)$$

and

$$\left.\frac{\partial \Psi_1}{\partial r}\right|_{r=r_c} = 2 r_c I_{P_1}(\mu). \quad (13b)$$

The general gas phase flow solution given by equation (12b) suggests an expansion for $u_1(\mu)$ of the form

$$u_1(\mu) = \sum_{n=0}^{\infty} u_{1n} P_n(\mu). \quad (13c)$$

The first order flow solution is finally obtained as

$$\Psi_1 = -\left[u_{10} I_{P_0}(\mu) + \{(k_1 + l_1 u_{11}) r^4 + (k_2 + l_2 u_{11}) r^2 + (k_3 + l_3 u_{11})/r + (k_4 + l_4 u_{11}) I_\Psi(r)\} I_{P_1}(\mu) + \sum_{n=2}^{\infty} u_{1n} f_n(r) I_{P_n}(\mu) \right] \quad (14)$$

where

$$k_1 = -2 r_c d_{12}$$
$$k_2 = -2 r_c d_{22}$$
$$k_3 = -(k_1 + k_2)$$
$$k_4 = -2 r_c d_{32}$$
$$l_1 = (2\phi_\eta + 1) d_{11} + d_{12}/r_c^2 - d_{13}/r_c^3$$
$$l_2 = (2\phi_\eta + 1) d_{21} + d_{22}/r_c^2 - d_{23}/r_c^3$$
$$l_3 = 1 - l_1 - l_2$$
$$l_4 = (2\phi_\eta + 1) d_{31} + d_{32}/r_c^2 - d_{33}/r_c^3$$

with d_{ij} the entries of the matrix $[D]$ which is defined as:

$$[D] = \begin{bmatrix} 5 & 3 + 2\phi_\eta & \left(\frac{1}{u_0^4} + \frac{1}{u_0^3} + \frac{\phi_\eta}{3u_0^2}\right) e^{-u_0} \\ 4r_c^3 + \frac{1}{r_c^2} & 2r_c + \frac{1}{r_c^2} & \frac{r_c^2}{u_0^4}(r_c + u_0) e^{-u_0/r_c} - \frac{I_\Psi(r_c)}{r_c} \\ r_c^2 - \frac{1}{r_c^3} & -\frac{1}{r_c^3} & \frac{1}{6u_0^2} e^{-u_0/r_c} + \frac{I_\Psi(r_c)}{r_c^2} \end{bmatrix}^{-1}$$

The separated first order equations for the S–Z variables are:

$$\frac{\partial}{\partial r}\left(r^2 \frac{\partial G_1}{\partial r}\right) + \frac{\partial}{\partial \mu}\left\{(1-\mu^2) \frac{\partial G_1}{\partial \mu}\right\} - v_0 \frac{\partial G_1}{\partial r} = -Sc \frac{\partial G_0}{\partial r} \frac{\partial \Psi_1}{\partial \mu}, \quad 1 < r < r_c \quad (15)$$

and

$$\frac{\partial}{\partial r}\left(r^2 \frac{\partial H_1}{\partial r}\right) + \frac{\partial}{\partial \mu}\left\{(1-\mu^2) \frac{\partial H_1}{\partial \mu}\right\} - v_0 \frac{\partial H_1}{\partial r} = -Sc \frac{\partial H_0}{\partial r} \frac{\partial \Psi_1}{\partial \mu}, \quad 1 < r < r_c. \quad (16)$$

The corresponding boundary conditions are:

$$\left.\frac{\partial G_1}{\partial r}\right|_{r=1} - v_0 G_1|_{r=1} = Sc(G_0|_{r=1} - \alpha_F) \sum_{n=0}^{\infty} u_{1n} P_n(\mu) \quad (17a)$$

$$\left.\frac{\partial H_1}{\partial r}\right|_{r=1} = Sc\, L \sum_{n=0}^{\infty} u_{1n} P_n(\mu) \quad (17b)$$

$$\left.\frac{\partial G_1}{\partial r}\right|_{r=r_c} + \left(Nu_0 - \frac{v_0}{r_c^2}\right) G_1\Big|_{r=r_c} = \left[\left\{\frac{Sc}{r_c^2} \sum_{n=0}^{\infty} u_{1n} P_n(\mu)\right\} - Nu_1\right](G_0|_{r=r_c} + Y_{X,\infty}) \quad (17c)$$

$$\left.\frac{\partial H_1}{\partial r}\right|_{r=r_c} + \left(Nu_0 - \frac{v_0}{r_c^2}\right) H_1|_{r=r_c} = \left[\frac{Sc}{r_c^2} \sum_{n=0}^{\infty} u_{1n} P_n(\mu) - Nu_1\right](H_0|_{r=r_c} - T_\infty + Y_{X,\infty}) \quad (17d)$$

$$G_1|_{r=1} = \phi_\beta H_1|_{r=1} \quad (17e)$$

where

$$\phi_\beta = (\beta G_0|_{r=1})/(H_0^2|_{r=1}).$$

A close look at the governing equations (15) and (16) and the boundary conditions (17a)–(17e) suggests that the variables G_1 and H_1 can be expanded in the following form:

$$G_1(r, \mu) = \sum_{n=0}^{\infty} R_{g_{1n}} P_n(\mu) \quad (18a)$$

and

$$H_1(r,\mu)=\sum_{n=0}^{\infty} R_{h_{1n}}P_n(\mu) \tag{18b}$$

where $P_n(\mu)$ are the Legendre polynomials of order n.

Substituting the above expansions into equations (15)–(17), the governing differential equations and boundary conditions for the radial functions, $R_{g_{1n}}$ and $R_{h_{1n}}$, can be obtained for each order of Legendre polynomial, $P_n(\mu)$. The equations associated with zero order Legendre polynomial are:

$$r^2R''_{g_{10}}+(2r-v_0)R'_{g_{10}}=Sc\,u_{10}G'_0 \tag{19}$$

and

$$r^2R''_{h_{10}}+(2r-v_0)R'_{h_{10}}=Sc\,u_{10}H'_0. \tag{20}$$

The general solutions of these equations can be expressed in matrix form as:

$$\begin{bmatrix}R_{g_{10}}\\ R_{h_{10}}\end{bmatrix}=\begin{bmatrix}C_{g_0}A_{g_{10}}B_{g_{10}}\\ C_{h_0}A_{h_{10}}B_{h_{10}}\end{bmatrix}\begin{bmatrix}f_{10}(r)\\ f_{20}(r)\\ f_{30}(r)\end{bmatrix} \tag{21}$$

where

$$C_{g_0}=-A_{g_0}Sc/v_0^2$$

$$C_{h_0}=-A_{h_0}Sc/v_0^2$$

$$f_{10}(r)=u_{10}\,e^{-v_0/r}(v_0/r+1)$$

$$f_{20}(r)=e^{-v_0/r}$$

$$f_{30}(r)=1.$$

It may be noted that $f_{10}(r)$ is the solution of the non-homogeneous part and $f_{20}(r)$, $f_{30}(r)$ are the two linearly independent solutions of the homogeneous part of equations (19) and (20). The integration constants $A_{g_{10}}$, $B_{g_{10}}$, $A_{h_{10}}$ and $B_{h_{10}}$ and the average enhancement in the evaporation velocity due to drop motion, u_{10}, can be evaluated from boundary conditions (17a)–(17e) separated to the order of $P_0(\mu)$. These are given by the expressions

$$A_{g_{10}}=0 \tag{22a}$$

$$A_{h_{10}}=\frac{C_{h_0}v_0^2\,e^{-v_0/r_c}}{Nu_0-v_0/r_c^2}\left[\frac{Nu_1\,v_0}{Sc\,r_c^2\,(Nu_0-v_0/r_c^2)}-Nu_0\,u_{10}\left\{1-\frac{1}{r_c}+\frac{1}{r_c^2(Nu_0-v_0/r_c^2)}\right\}\right] \tag{22b}$$

$$B_{g_{10}}=C_{g_0}v_0\left[\frac{Nu_1\,v_0^2}{Sc\,r_c^2\,Nu_0(Nu_0-v_0/r_c^2)}+u_{10}\left\{1+\frac{v_0}{r_c}-\frac{v_0}{Nu_0\,r_c^2}-\frac{v_0^2}{Nu_0\,r_c^4(Nu_0-v_0/r_c^2)}\right\}\right] \tag{22c}$$

$$B_{h_{10}}=C_{h_0}v_0u_{10}(v_0+1) \tag{22d}$$

$$u_{10}=\frac{Nu_1}{Sc\,r_c\,Nu_0(Nu_0-v_0/r_c^2)}\,\frac{v_0}{r_c-1+r_c/(Nu_0r_c-v_0^2)}. \tag{22e}$$

The governing equations of the radial functions separated to the first order Legendre polynomial are

$$r^2R''_{g_{11}}+(2r-v_0)R'_{g_{11}}-2R_{g_{11}}=Sc\,G'_0\{(k_1+l_1u_{11})r^4+(k_2+l_2u_{11})r^2+(k_3+l_3u_{11})/r+(k_4+l_4u_{11})I_\Psi(r)\},\quad 1<r<r_c \tag{23}$$

and

$$r^2R''_{h_{11}}+(2r-v_0)R'_{h_{11}}-2R_{h_{11}}=Sc\,H'_0\{(k_1+l_1u_{11})r^4+(k_2+l_2u_{11})r^2+(k_3+l_3u_{11})/r+(k_4+l_4u_{11})I_\Psi(r)\},\quad 1<r<r_c. \tag{24}$$

The general solutions of the above equations are given by

$$\begin{bmatrix}R_{g_{11}}\\ R_{h_{11}}\end{bmatrix}=\begin{bmatrix}C_{g_1} & A_{g_{11}} & B_{g_{11}}\\ C_{h_1} & A_{h_{11}} & B_{h_{11}}\end{bmatrix}\begin{bmatrix}f_{11}(r)\\ f_{21}(r)\\ f_{31}(r)\end{bmatrix} \tag{25}$$

where

$$f_{11}(r)=(k_1+l_1u_{11})\left\{r^3\,e^{-v_0/r}(r^2-\tfrac{5}{6}v_0r+\tfrac{1}{3}v_0^2)-2v_0^4(2r-v_0)\int_{1/v_0}^{r/v_0}\xi^3\,e^{-1/\xi}\,d\xi\right\}+\left\{(k_2+l_2u_{11})v_0^2r+(k_3+l_3u_{11})\left(\frac{6r}{v_0}+3-\frac{v_0}{2r^2}\right)\right\}e^{-v_0/r}+(k_4+l_4u_{11})\left[(2r-v_0)\int_1^r\frac{1}{\xi^2}(2\xi+v_0)\,e^{-v_0/\xi}\,I_\Psi(\xi)\,d\xi-(2r+v_0)\,e^{-v_0/r}\int_1^r\frac{1}{\xi^2}(2\xi-v_0)I_\Psi(\xi)\,d\xi\right]$$

$$f_{21}(r)=2r-v_0$$

$$f_{31}(r)=e^{-v_0/r}(2r+v_0).$$

The integration constants $A_{g_{11}}$, $A_{h_{11}}$, $B_{g_{11}}$ and $B_{h_{11}}$ and the velocity coefficient, u_{11}, can be evaluated following a similar procedure as discussed in the context of radial solutions associated with the zero order Legendre polynomial. Expressions for C_{g_1} and C_{h_1} as well as the aforementioned constants are given in Appendix B.

The governing equations for the radial functions associated with Legendre polynomials of order $n\geqslant 2$ are given by:

$$r^2R''_{g_{1n}}+(2r-v_0)R'_{g_{1n}}-n(n+1)R_{g_{1n}}=Sc\,G'_0u_{1n},\quad 1<r<r_c \tag{26}$$

and

$$r^2R''_{h_{1n}}+(2r-v_0)R'_{h_{1n}}-n(n+1)R_{h_{1n}}=Sc\,H'_0u_{1n},\quad 1<r<r_c. \tag{27}$$

An examination of the above equations reveals that the solutions $R_{g_{1n}}$ and $R_{h_{1n}}$ will contain u_{1n} only as a

multiplicative constant. Substitution of such solutions into the five boundary conditions derived from equations (17a) to (17e) leads to the cancellation of u_{1n} from all the equations (when $u_{1n} \neq 0$). This results in a system of five linearly independent algebraic equations for determining the four integration constants $A_{g_{1n}}$, $B_{g_{1n}}$, $A_{h_{1n}}$ and $B_{h_{1n}}$. Such a system permits only a trivial solution for the aforementioned constants and u_{1n}. Therefore, the solutions of the S–Z variables and the stream functions corresponding to Legendre functions of order $n \geqslant 2$ are identically equal to zero.

NUMERICAL EVALUATION OF THE SOLUTIONS AND DETERMINATION OF PHYSICAL QUANTITIES

The closed-form solutions derived in the previous section were verified against finite difference solutions of the corresponding separated equations. In order to match these two solutions, it was found to be necessary to accurately evaluate the integral, $I_\Psi(r)$ in equation (12b) and the integrals contained in the definition of $f_{11}(r)$ in equation (25). These were computed using a fourth order Gauss–Legendre quadrature, coupled with fourth order Lagrangian interpolation where necessary.

For a given set of problem parameters, numerical computations for the velocity coefficients and the S–Z variables were performed first. These results were further processed to extract physical quantities such as the flame shape and the profiles of temperature, fuel concentration and oxidizer concentration. The procedure adopted for the evaluation of various physical quantities is described briefly below.

The evaporation velocity at a particular angular position on the drop surface can be obtained from the velocity coefficients using the expression

$$u_d(\mu) = u_0 + Re[u_{10}P_0(\mu) + u_{11}P_1(\mu)]. \quad (28)$$

The velocity coefficients u_0, u_{10} and u_{11} are, in turn, given by equations (10c), (22e) and (B5). In particular, equation (10c), which determines the spherically symmetric evaporation velocity, u_0, is transcendental in nature. In the present study, this equation has been solved using the bisection method.

The location of the flame at each angular position, $r_f(\mu)$, is identified as the point where the variable G attains zero value. In order to retrieve the temperature and concentration profiles from the solutions of the S–Z variables, it is necessary to invoke the thin-flame approximation. By virtue of this approximation, it can be shown that

$$Y_F = G, \quad Y_X = 0 \quad \text{and} \quad T = H \quad \text{for} \quad 1 \leqslant r \leqslant r_f \quad (29a)$$

and

$$Y_F = 0, \quad Y_X = -G \quad \text{and} \quad T = H - G \quad \text{for} \quad r > r_f. \quad (29b)$$

It may be noted here that the evaporation velocity u_d can be evaluated as discussed earlier, even in the pure evaporation situation when the flame is absent, if $Y_X \cong 0$ near $r = 1$ and $Y_F \cong 0$ towards the cell surface. However, the extraction of temperature and concentration fields from the S–Z solutions is possible only when there is an envelope flame within the cell.

RESULTS AND DISCUSSION

Validation of the cell model for spray combustion analysis

In order to validate the analytical results and the use of the cell model, attempts have been made to recover the known solutions of earlier studies in some limiting cases. These comparisons are described below.

(i) For $Re = 0$ and in the limit $r_c \to \infty$, the present problem reduces to the case of a stationary, isolated droplet burning in a quiescent atmosphere. The corresponding expressions for the burning rate and the flame stand-off ratio (r_f/r_d) match with equations (3.58) and (3.62) of ref. [25].

(ii) Analytical studies are also available for various arrangements of stationary droplets [14–17, 19]. Some of their results for the evaporation velocity have been compared with our predictions in Fig. 2. The results of the earlier studies corresponding to a two-droplet array, four droplets placed in a square arrangement and eight droplets in a cubical arrangement have been included in the figure. For the sake of comparison, the cell radius has been assumed to be equal to half the droplet spacing while obtaining the results of the present cell model. Also, the Nusselt number values used in the figure were selected on the basis of the expressions provided in Appendix A.

The predictions for different droplet arrangements

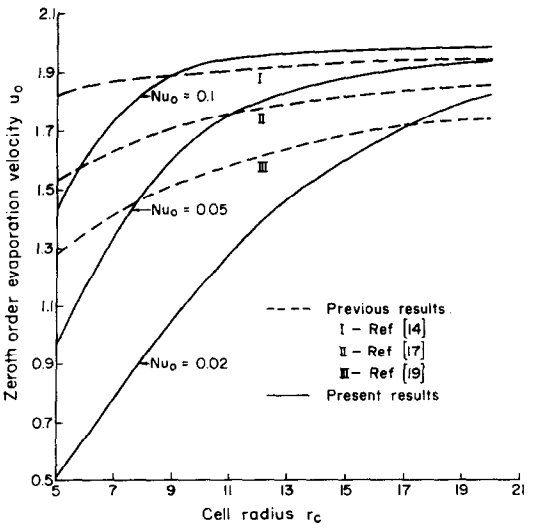

FIG. 2. Comparison between cell model results and previous analytical results for specific droplet arrangements.

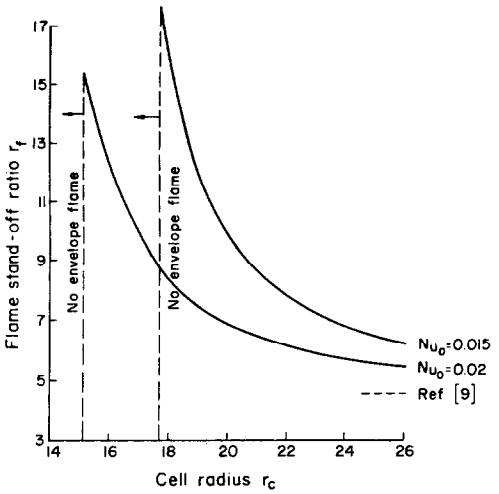

FIG. 3. Variation of flame stand-off ratio with cell radius and cell Nusselt number for spherically symmetric burning.

in Fig. 2 indicate a decrease in evaporation velocity as the number of droplets increases. It may be noted that the present formulation corresponds to the arrangement in which a typical droplet is surrounded by a large number of droplets from all sides. Therefore, as expected, our results for evaporation velocity fall below those for a limited number of droplets. With respect to droplet spacing, the trends exhibited are similar for the previous as well as the present analyses. Both indicate that the evaporation velocity increases with r_c due to the increased availability of oxygen. For large r_c, the cell model results merge with those of the earlier studies, with all the curves approaching the limiting value for an isolated droplet. For low r_c, the predictions of the present study are considerably lower than those of the selected droplet configurations. This discrepancy can be explained from the fact that in the earlier studies, all the droplets are on the boundary of the droplet cluster and, therefore, are subjected to only partial asphyxiation. In the cell model, however, a typical droplet is always an interior one, which is surrounded by neighbours all around.

(iii) The variation of flame stand-off ratio with cell radius and Nu_0 is shown in Fig. 3, along with a comparison of the present results with the prediction of Fendell *et al.* [9] for the burning of an isolated droplet when $Re = 0$. Except for r_c and Nu_0, which are particular to the present study, values of all the other parameters have been taken from ref. [9]. For $Nu_0 \sim 0.02$ and $r_c \to \infty$, the flame stand-off ratio predicted by the present approach compares favourably with that of Fendell and co-workers. It is observed that the flame moves away from the droplet surface as the droplet spacing is reduced. There seems to be a tendency for the flame to position itself suitably so that it receives the appropriate supply of oxygen. At each value of Nu_0, for r_c less than a critical value, no envelope flame exists. It is surmised that for such dense sprays, the combustion may no longer be governed by the discrete droplet burning mode and may correspond to a group burning regime.

(iv) In order to evaluate the performance of the cell model in the presence of drop motion, our results for large r_c have been compared with those of Fendell *et al.* [9] in Tables 1 and 2. The values of $Nu_0 = 0.05$ and $r_c = 25$ have been used to obtain the cell model results shown in these tables. Table 1 provides a comparison between the velocity coefficients, while the flame location at two different Reynolds numbers is compared in Table 2 for various angles. The agreement between the results is satisfactory.

The novel contribution of the present study lies in the development of results for multi-drop situations in the presence of convection. The comparisons provided here illustrate that when the droplet spacing or the Reynolds number is varied, the cell model results indeed approach appropriate limits. For spray combustion in the discrete droplet burning mode, therefore, the cell model offers a powerful mathematical tool. Some important results for multi-droplet combustion including convective effects are presented in the following sections.

Evaporation velocity coefficients

In Figs. 4 and 5, the velocity coefficients, u_0, u_{10} and u_{11}, are plotted against the cell radius for different Nu_0 and cloud conditions. It is important to note that u_0 gives the evaporation velocity in the absence of drop motion, while u_{10} and u_{11} represent the average enhancement and the amplitude of angular variation respectively due to drop motion. In the context of separating the convective effects to different orders of Reynolds number, the variation in Nu_0 can be interpreted in terms of the variation in the heat/mass capacity of the convective cloud at the cell boundary.

In both the figures, the results for the lower range of cell radius correspond to the pure evaporation situation. As the cell radius is increased, u_0 increases due to the higher rate of oxygen transfer at the cell surface. It may be noted from equation (9c) that the mass transfer is influenced by two factors, namely, the Nusselt number Nu_0 and the strength of the radially out-

Table 1.

	u_0	u_{10}	u_{11}
Ref. [9]	1.942	0.971	0.715
Present study	1.956	0.839	0.527

Table 2.

	$Re = 0.0$	$Re = 0.1$		
	All angles	$\theta = 0°$	$\theta = 90°$	$\theta = 180°$
Ref. [9] r_f	4.60	3.89	4.05	4.49
Present study r_f	4.49	3.64	3.94	4.36

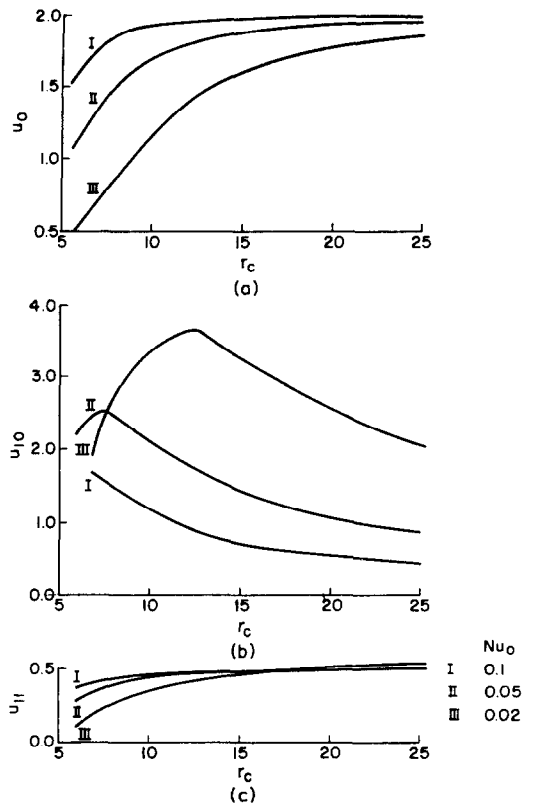

FIG. 4. Effects of cell radius and cell Nusselt number on evaporation velocity coefficients.

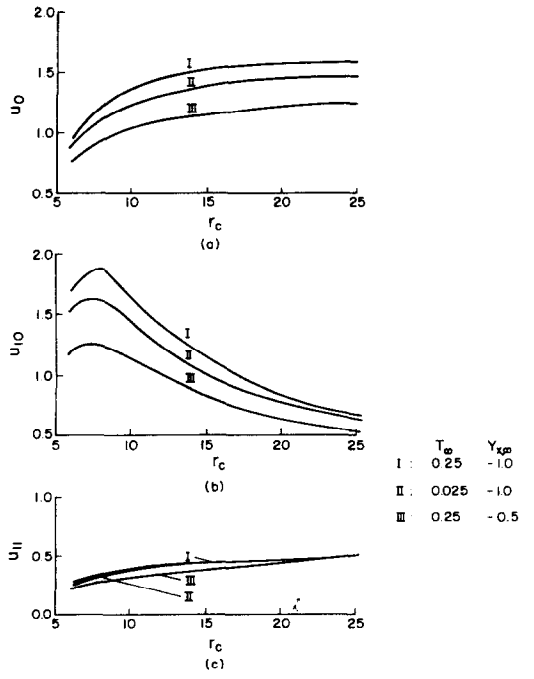

FIG. 5. Effects of cloud conditions on the evaporation velocity coefficients.

ward flow field. Indeed, the radially outward flow tends to oppose the oxygen transfer to the cell. For larger cell radius, the effect of radial flow on transport decreases in comparison to that of the convective cloud Nusselt number; further, the cell surface area is also larger. Both factors contribute to the increase in u_0 with r_c. For a fixed cell radius, u_0 increases with Nu_0 as the effectiveness of the cloud in transferring mass is enhanced. The arguments cited above with regard to the rate of oxygen transfer at the cell surface are applicable when combustion takes place within the cell. For the pure evaporation situation, similar arguments may be put forth for the transfer of fuel to the cloud through the mixture of fuel, oxygen and inert species.

The average enhancement in the evaporation velocity, u_{10}, has a complex dependence on the cell radius and Nu_0, as can be seen from equation (22e). For low r_c, which generally corresponds to the evaporation situation, the enhancement increases due to increase in the zero order flow field. It is to be borne in mind that in this case the rate of fuel transfer is aided by the radially outward flow. However, in the combustion regime corresponding to large r_c, the opposing effect of the zero order field to oxygen transport leads to a reduction in the average enhancement. The amplitude of angular variation in the evaporation velocity, u_{11}, is not significantly affected by either the cell radius or the Nusselt number.

With regard to the effects of cloud conditions upon the velocity coefficients, it is observed that the oxygen concentration of the cloud influences the rate of evaporation much more strongly than the cloud temperature (Fig. 5). This is to be expected, since fuel drops are likely to suffer more from paucity of oxygen than from heat in a multi-drop combustion situation. The mass transfer process thus appears to be the controlling mechanism.

Flame shapes for quasi-steady burning

The flame shapes at various Reynolds numbers and droplet spacings are presented in Fig. 6. In order to provide a comparison between the relative sizes of the drop and the flame, the droplet has been shown as a hatched surface. Also, at each Reynolds number, the range of droplet spacing for which no envelope flame exists has been indicated.

The flame shifts outwards when the droplet spacing is reduced. It may be inferred here that in the oxygen-starved environment within the cell, the flame locates itself as close to the cell surface as is necessary, where the oxygen requirement of the flame is met. In the oxygen-rich environment corresponding to a large cell radius, it is plausible that the flame location is controlled by the demand for fuel. The flame shape results of the present study smoothly approach the prediction of Fendell *et al.* [9] for isolated droplet burning. At higher Reynolds number, the flame is drawn closer to the drop in the front, and pushed further away from the drop in the rear portion, with respect to the direc-

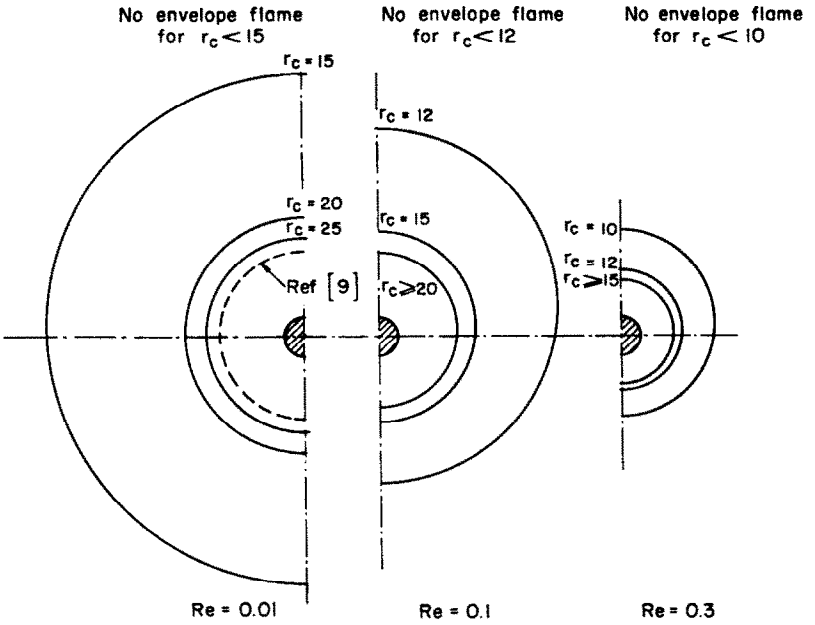

FIG. 6. Flame shapes for different Reynolds numbers and droplet spacings.

tion of the drop motion. Also, the overall flame location advances nearer to the drop, which appears to be a consequence of increased oxygen supply, in the light of the arguments presented above. An important effect of the increase in Reynolds number is to lower the threshold cell radius above which an envelope flame exists. It is interesting to note that the flame shapes predicted by the regular perturbation analysis are smooth and exhibit no apparent anomaly, even at the fairly high value of Reynolds number of 0.3. However, at the same *Re*, the flame shape, determined on the basis of the singular perturbation study of Fendell *et al.* [9], indicated a breakdown of the analysis.

Temperature and concentration profiles

The profiles of gas phase temperature and mass fractions of oxygen and fuel are shown in Figs. 7(a), (b), 8 and 9. In Fig. 7, the effects of the cell size and the angular position are shown, while those of convective cloud conditions are depicted in Figs. 8 and 9. These profiles have been drawn against the normalized radial position defined by

$$\xi = (r - r_d)/(r_c - r_d).$$

In all the figures, the flame location is marked by a sharp discontinuity in the temperature as well as in the concentration profiles. This is a consequence of the thin-flame approximation invoked in the present analysis. In addition, due to the same approximation, the region between the drop and the flame is devoid of oxygen and the region beyond the flame is devoid of fuel. It is observed that the temperature and the fuel fraction at the drop surface exhibit only mild variations over the range of parameters considered here; the temperature and the oxygen concentration at the cell surface, on the other hand, show significant variation for different conditions. The near-constancy of drop surface conditions reaffirms the usual observation that the wet bulb temperature is close to the boiling point of the fuel.

The oxygen concentration in the cloud, in general, appears to have a much stronger influence upon the profiles than the cloud temperature (see Figs. 8 and 9). This observation supports our claim that the transfer of oxygen plays a crucial role in spray combustion. The curves corresponding to $\bar{Y}_{X,\infty} = 1.0$ and $\bar{Y}_{X,\infty} = 0.7$ represent the burning of the droplet in an oxygen-rich atmosphere. In such a situation, the most notable change observed is in the flame temperature, when the oxygen concentration of the cloud is varied. For oxygen-starved situations, however, the profiles of temperature and concentration and the flame location undergo drastic changes with oxygen concentration of the cloud. An interesting trend of slight shift in the flame location closer to the drop is observed when $\bar{Y}_{X,\infty}$ changes from 1.0 to 0.7. It is conjectured that this shift may be due to the change in the flame temperature, which affects the evaporation process at the drop surface.

CONCLUSION

A mathematical solution to the spray combustion problem including convective effects due to drop motion, has been developed. The validity of the results have been critically examined and established by comparing with other works in the literature for various limiting cases. The effects of droplet spacing, drop motion and the condition of the spray environment

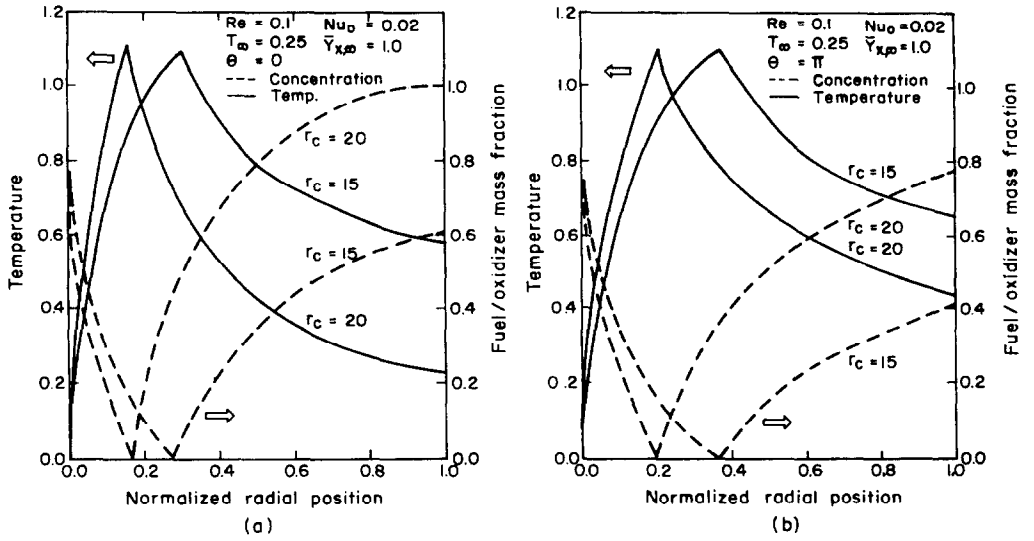

FIG. 7. Variation of temperature and concentration profiles along the axis.

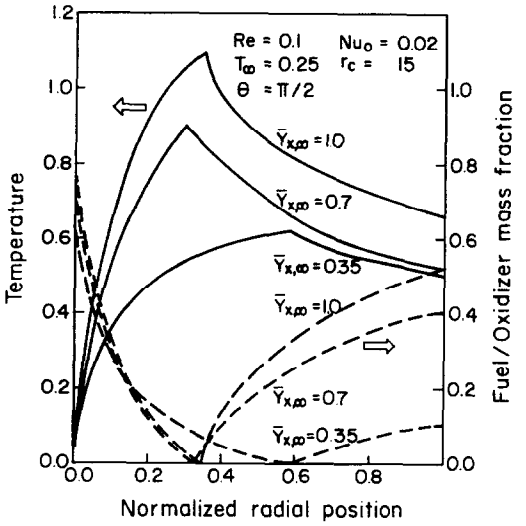

FIG. 8. Temperature and concentration profiles for different oxidizer concentrations in the cloud.

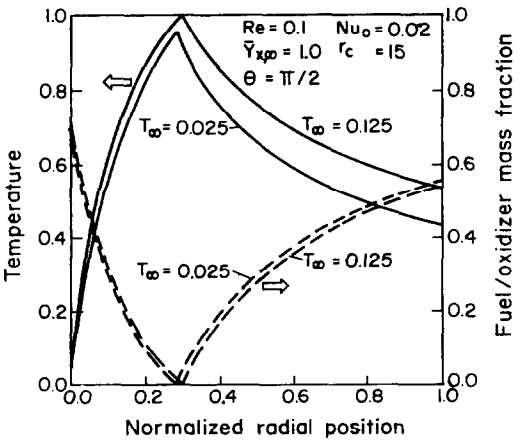

FIG. 9. Temperature and concentration profiles for different cloud temperatures.

upon the combustion characteristics have been highlighted.

REFERENCES

1. G. A. E. Godsave, Studies of the combustion of drops in a fuel spray: the burning of single drops of fuel, *Proc. 4th Symp. (Int.) on Combustion*, Combustion Institute, pp. 818–830 (1953).
2. C. H. Waldman, Theory of non-steady droplet combustion, *Proc. 15th Symp. (Int.) on Combustion*, Combustion Institute, pp. 429–441 (1975).
3. C. K. Law, S. H. Chung and N. Srinivasan, Gas-phase quasi-steadiness and fuel vapour accumulation effects in droplet burning, *Combust. Flame* **38**, 173–198 (1980).
4. G. M. Faeth, Current status of droplet and liquid combustion, *Prog. Energy Combust. Sci.* **3**, 191–244 (1977).
5. S. Prakash and W. A. Sirignano, Liquid fuel droplet heating with internal circulation, *Int. J. Heat Mass Transfer* **21**, 885–895 (1978).
6. S. Prakash and W. A. Sirignano, Theory of convective droplet vaporization with unsteady heat transfer in the circulating liquid phase, *Int. J. Heat Mass Transfer* **23**, 253–268 (1980).
7. G. Gogos and P. S. Ayyaswamy, A model for the evaporation of a slowly moving droplet, *Combust. Flame* **74**, 111–129 (1988).
8. G. Gogos, S. Sadhal, P. S. Ayyaswamy and T. Sundararajan, Thin-flame theory for the combustion of a moving liquid drop; effects due to variable density, *J. Fluid Mech.* **171**, 121–144 (1986).
9. F. E. Fendell, M. L. Sprankle and D. S. Dodson, Thin-flame theory for a fuel droplet in slow viscous flow, *J. Fluid Mech.* **26**, 267–280 (1966).
10. J. J. Sangiovanni, A model for the nonsteady ignition and combustion of a fuel droplet. In *Advances in Chemistry Series*, 166, *Evaporation Combustion of Fuels* (Edited by J. T. Zung), pp. 27–53. American Chemical Society, Washington, DC (1978).
11. T. Suzuki and H. H. Chiu, Multi-droplet combustion of liquid propellants, *Proc. 9th (Int.) Symp. Space Technol. Sci.*, pp. 145–154 (1971).
12. H. H. Chiu and T. M. Liu, Group combustion of liquid droplets, *Combust. Sci. Technol.* **17**, 127–142 (1977).
13. H. H. Chiu, H. Y. Kim and E. I. Croke, Internal group combustion of liquid droplets, *Proc. 19th Symp. (Int.) on Combustion*, Combustion Institute, pp. 971–980 (1983).

14. T. A. Brzustowski, E. M. Twardus, S. Wojcicki and A. Sobeislak, Interaction of two burning fuel droplets of arbitrary size, *AIAA J.* **27,** 1234–1242 (1979).
15. M. Labowsky, The effects of nearest neighbour interactions on the evaporation rate of cloud particles, *Chem. Engng Sci.* **31,** 803–813 (1976).
16. M. Labowsky, Transfer rate calculations for compositionally dissimilar interacting particles, *Chem. Engng Sci.* **35,** 1041–1048 (1980).
17. M. Labowsky, Calculation of burning rates of interacting fuel droplets, *Combust. Sci. Technol.* **22,** 217–226 (1980).
18. A. K. Ray and E. J. Davis, Heat and mass transfer with multiple particle interactions. Part I. Droplet evaporation, *Chem. Engng Commun.* **6,** 61–79 (1980).
19. M. Marberry, A. K. Ray and K. Leung, Effect of particle interactions on burning droplets, *Combust. Flame* **57,** 237–245 (1984).
20. J. Happel, Viscous flow in multiparticle systems: slow motion of fluids relative to beds of spherical particles, *A.I.Ch.E. Jl* **4,** 197–201 (1958).
21. S. Kuwabara, The forces experienced by randomly distributed parallel circular cylinders or spheres in a viscous flow at small Reynolds number, *J. Phys. Soc. Japan* **14,** 527–532 (1959).
22. J. T. Zung, Evaporation rate and lifetimes of clouds and sprays in air—the cellular model, *J. Chem. Phys.* **46,** 2064–2070 (1967).
23. J. M. Tishkoff, A model for the effect of droplet interactions on vaporization, *Int. J. Heat Mass Transfer* **22,** 1407–1415 (1979).
24. J. Bellan and R. Cuffel, A theory of nondilute spray evaporation based upon multiple droplet interaction, *Combust. Flame* **51,** 55–67 (1983).
25. F. A. Williams, *Combustion Theory.* Benjamin/Cummings, Monelo Park, California (1985).
26. B. Gal-or and S. Waslo, Hydrodynamics of an ensemble of drops (or bubbles) in the presence or absence of surfactants, *Chem. Engng Sci.* **23,** 1431–1446 (1968).
27. M. M. El-Kaissy and G. M. Homsy, A theoretical study of pressure drop and transport in packed beds at intermediate Reynolds numbers, *Ind. Engng Chem. Fundam.* **12,** 82–88 (1973).
28. R. Clift, J. R. Grace and M. E. Weber, *Bubbles Drops and Particles.* Academic Press, New York (1978).
29. S. S. Sadhal and P. S. Ayyaswamy, Flow past a liquid drop with a large non-uniform radial velocity, *J. Fluid Mech.* **133,** 65–81 (1983).

APPENDIX A

For obtaining the order of magnitude for the zero order Nusselt number, Nu_0, we shall consider the auxiliary problem of heat transfer in a purely radial flow field. The dimensionless governing equation for temperature is

$$(r^2T')'-v_0T'=0 \tag{A1}$$

where $T=T(r)$ only.

The general solution of the above equation is

$$T=A\exp(-v_0/r)+B:$$

subjected to the boundary conditions

$$T=T_c \quad \text{at} \quad r=r_c$$

and

$$T\to T_\infty \quad \text{as} \quad r\to\infty$$

the final solution of temperature becomes

$$T=\frac{\exp(-v_0/r)-1}{\exp(-v_0/r_c)-1}(T_c-T_\infty)+T_\infty. \tag{A2}$$

The Nusselt number at the surface $r=r_c$ can then be determined from the heat balance relation:

$$[-\mathrm{d}T/\mathrm{d}r+(T-T_\infty)v_0/r^2]|_{r=r_c}=Nu(T_c-T_\infty) \tag{A3}$$

where $Nu=hr_d/\lambda$.

Combining equations (A2) and (A3), it is finally obtained that

$$Nu|_{r=r_c}=\frac{v_0}{r_c^2}[\{\exp(v_0/r_c)-1\}^{-1}+1]. \tag{A4}$$

For pure conduction, in the limit of $v_0\to 0$, the above equation reduces to

$$Nu|_{r=r_c}=1/r_c. \tag{A5}$$

If the radial field is such that $v_0\ll r_c$, then one obtains the Nusselt number to the leading order of (v_0/r_c) as

$$Nu|_{r=r_c}=(1+v_0/2r_c)/r_c. \tag{A6}$$

Now, putting $r_c=20$, the conduction limit Nusselt number is calculated from equation (A5) as

$$Nu=0.05.$$

In the range of validity of equation (A6), the value of Nu is slightly larger. For the multi-drop burning problem, equations (A4)–(A6) can be employed as guidelines for selecting the range of Nu_0, by taking $r=r_c$ to represent the cell surface.

APPENDIX B

The expressions for the integration constants C_{g_1}, C_{h_1}, $A_{g_{11}}$, $B_{g_{11}}$ and $B_{h_{11}}$ of equation (25) and the velocity coefficient, u_{11}, are given below:

$$C_{g_1}=-C_{g_0}/v_0$$

$$C_{h_1}=-C_{h_0}/v_0$$

$$A_{g_{11}}=\frac{1}{\Delta_1}\{g_{22}(a_{11}u_{11}+a_{12})-g_{12}(a_{21}u_{11}+a_{22})\} \tag{B1}$$

$$A_{h_{11}}=\frac{1}{\Delta_2}\{h_{22}(b_{11}u_{11}+b_{12})-h_{12}(b_{21}u_{11}+b_{22})\} \tag{B2}$$

$$B_{g_{11}}=\frac{1}{\Delta_1}\{g_{11}(a_{21}u_{11}+a_{22})-g_{21}(a_{11}u_{11}+a_{12})\} \tag{B3}$$

$$B_{h_{11}}=\frac{1}{\Delta_2}\{h_{11}(b_{21}u_{11}+b_{22})-h_{21}(b_{11}u_{11}+b_{12})\} \tag{B4}$$

and

$$\begin{aligned}u_{11}=&[(2-v_0)\{\phi_\beta(b_{12}h_{22}-b_{22}h_{12})/\Delta_2\\&-(a_{12}g_{22}-a_{22}g_{12})/\Delta_1\}\\&+\mathrm{e}^{-v_0}(2+v_0)\{\phi_\beta(b_{22}h_{11}-b_{12}h_{21})/\Delta_2\\&-(a_{22}g_{11}-a_{12}g_{21})/\Delta_1\}\\&+\mathrm{e}^{-v_0}(\phi_\beta C_{h_1}-C_{g_1})\{k_1(1-5v_0/6\\&+v_0^2/3)+k_2v_0^2\\&+k_3(6/v_0+3-v_0^2/2)\}][(2-v_0)\\&\times\{(a_{11}g_{22}-a_{21}g_{12})/\Delta_1\\&-\phi_\beta(b_{11}h_{22}-b_{21}h_{12})/\Delta_2\}\\&+\mathrm{e}^{-v_0}(2+v_0)\{(a_{21}g_{11}-a_{11}g_{21})/\Delta_1\\&-\phi_\beta(b_{21}h_{11}-b_{11}h_{21})/\Delta_2\}\\&+\mathrm{e}^{-v_0}(C_{g_1}-\phi_\beta C_{h_1})\{l_1(1-5v_0/6\\&+v_0^2/3)+l_2v_0^2+l_3(6/v_0+3-v_0^2/2)\}]^{-1}\end{aligned} \tag{B5}$$

where

$$g_{11} = v_0^2 - 2v_0 + 2$$

$$h_{11} = 2$$

$$g_{12} = 2e^{-v_0}$$

$$h_{12} = e^{-v_0}(v_0^2 + 2v_0 + 2)$$

$$g_{21} = h_{21} = (Nu_0 - v_0/r_c^2)(2r_c - v_0) + 2$$

$$g_{22} = h_{22} = e^{-v_0/r_c}\{Nu_0(2r_c + v_0) + 2\}$$

$$\Delta_1 = g_{11}g_{22} - g_{12}g_{21}$$

$$\Delta_2 = h_{11}h_{22} - h_{12}h_{21}$$

$$a_{11} = C_{g_1} e^{-v_0}\{v_0^2 - (1 - 4v_0/3 + v_0^2)I_1 - v_0^2 I_2 - (6/v_0 + v_0^2)I_3\}$$

$$b_{11} = C_{h_1} e^{-v_0}\{v_0^2 - (1 - v_0/3 + v_0^2/6 + v_0^3/3)I_1 - v_0^2(v_0 + 1)I_2 - (6/v_0 + 6 + 3v_0 + v_0^2 + v_0^3/2)I_3\}$$

$$a_{12} = -C_{g_1} e^{-v_0}\{(1 - 4v_0/3 + v_0^2)k_1 + v_0^2 k_2 + (6/v_0 + v_0^2)k_3\}$$

$$b_{12} = -C_{h_1} e^{-v_0}\{(1 - v_0/3 + v_0^2/6 + v_0^3/3)k_1 + v_0^2(v_0 + 1)k_2 + (6/v_0 + 6 + 3v_0 + v_0^2 + v_0^3/2)k_3\}$$

$$a_{21} = Sc\, v_0(\alpha_F + Y_{X,\infty})/(Nu_0 r_c^4) - C_{g_1}\sum_{i=1}^{4} l_i n_i$$

$$b_{21} = -Sc\, Lv_0 e^{v_0(1 - 1/r_c)}\{r_c^4(Nu_0 - v_0/r_c^2)\}^{-1} - C_{h_1}\sum_{i=1}^{4} l_i n_i$$

$$a_{22} = -C_{g_1}\sum_{i=1}^{4} k_i n_i$$

$$b_{22} = -C_{h_1}\sum_{i=1}^{4} k_i n_i$$

$$n_1 = \{r_c^2(r_c^2 - 4v_0 r_c/3 + v_0^2) + Nu_0 r_c^3(r_c^2 - 5v_0 r_c/6 + v_0^2/3)\} e^{-v_0/r_c} - 2v_0^4\{(Nu_0 - v_0/r_c^2)(2r_c - v_0) + 2\}\int_{1/r_0}^{r_c/r_0} \xi^3 e^{-1/\xi}\, d\xi$$

$$n_2 = v_0^2 e^{-v_0/r_c}(Nu_0 r_c + 1)$$

$$n_3 = e^{-v_0/r_c}\{2(6r_c^3 + v_0^3) + Nu_0 r_c(12r_c^3 + 6v_0 r_c^2 - v_0^3)\}/(2v_0 r_c^3)$$

$$n_4 = g_{21}\int_1^{r_c} \frac{1}{\xi^2}(2\xi + v_0) \times e^{-v_0/\xi} I_\Psi(\xi)\, d\xi - g_{22}\int_1^{r_c} \frac{1}{\xi^2} \times (2\xi - v_0) I_\Psi(\xi)\, d\xi.$$

MODELE ANALYTIQUE DE LA COMBUSTION DE GOUTTELETTES PULVERISEES DE COMBUSTIBLE, LENTEMENT MOBILES

Résumé—La combustion d'un aérosol de combustible dilué a été analysée dans le cadre d'un modèle de cellules sphériques. La combustion quasi permanente d'une gouttelette typique a été étudiée dans l'approximation de la flamme mince. A la surface de la cellule, on impose les conditions aux limites de tension de cisaillement nulle et de transfert convectif de chaleur et de masse nul. Des solutions analytiques pour le mouvement rampant de la goutte ont été obtenues par une procédure de perturbation régulière avec le nombre de Reynolds de la goutte comme paramètre de perturbation. Une étude paramétrique est faite qui implique le nombre de Reynolds, la taille de la cellule et les conditions d'écoulement libre au delà de la surface de la cellule.

EIN ANALYTISCHES MODELL FÜR DIE SPRÜHNEBELVERBRENNUNG BEI BRENNSTOFFTROPFEN GERINGER GESCHWINDIGKEIT

Zusammenfassung—Es wird die Verbrennung eines verdünnten Brennstoff-Sprühnebels mit Hilfe eines Kugelzellenmodells untersucht. Das stationäre Brennen eines typischen Tröpfchens wird mit Hilfe einer speziellen Näherung beschrieben. An der Zelloberfläche werden folgende Randbedingungen aufgeprägt: verschwindende Schubspannung und verschwindender konvektiver Wärme- und Stofftransport. Für die schleichende Bewegung der Tropfen ergeben sich unter Anwendung eines Störungsverfahrens mit der Tropfen-Reynolds-Zahl als Störungsparameter analytische Lösungen. Abschließend werden Parameteruntersuchungen für die Tropfen-Reynolds-Zahl, die Zellgröße und die Freistrombedingungen außerhalb der Zelloberfläche durchgeführt.

АНАЛИТИЧЕСКАЯ МОДЕЛЬ ГОРЕНИЯ РАСПЫЛА ТОПЛИВА ПРИ МЕДЛЕННОМ ДВИЖЕНИИ КАПЕЛЬ

Аннотация—Горение разжиженного распыла топлива анализируется в рамках сферической ячеистой модели. Квазистационарное горение типичной капли исследовалось с помощью аппроксимации тонкого пламени. На поверхности ячейки используются граничные условия нулевого напряжения сдвига и конвективного тепло- и массопереноса. Методом регулярных возмущений с числом Рейнольдса для капли в качестве параметра возмущения получены аналитические решения для ползущего движения капли. Выполнено также параметрическое исследование с использованием числа Рейнольдса, размера ячейки и условий свободного течения за пределами ее поверхности.